CDX2-UPK1B-PIK3IP1-PI3K/AKT signaling axis regulates gastric cancer cell invasion and migration and influences patient prognosis

SHAODONG ZHONG[1], HENG ZHANG[2] and JIN HUANG[1]

[1]Gastroenterology/Endoscopy Clinic, The First Affiliated Hospital of University of Science and Technology of China (Anhui Provincial Tumor Hospital), Division of Life Science and Medicine, University of Science and Technology of China, Hefei, Anhui 230031, P.R. China; [2]Department of Women and Children Radiotherapy, The First Affiliated Hospital of USTC (Anhui Provincial Tumor Hospital), Division of Life Science and Medicine, University of Science and Technology of China, Hefei, Anhui 230031, P.R. China

Received September 2, 2025; Accepted January 23, 2026

DOI: 10.3892/etm.2026.13179

Abstract. Gastric cancer (GC) remains one of the leading causes of cancer-related mortality worldwide, with malignant metastasis being a major determinant of patient prognosis. The metastatic process involves a number of phenotypic alterations, including enhanced invasive and migratory capacities. The growing availability of unbiased transcriptomic data has facilitated the identification of metastasis-associated molecular biomarkers and has enabled the exploration of their underlying mechanisms, with the aim of identifying novel therapeutic targets. In the present study, differential expression analysis was performed using The Cancer Genome Atlas Stomach Adenocarcinoma dataset to identify genes associated with malignant metastasis in GC. Prognostic signature genes were subsequently identified using Least Absolute Shrinkage and Selection Operator and Cox regression analyses. Western blotting, wound healing and Transwell assays were performed to investigate the association between gene expression, PI3K/AKT signaling activity, and GC cell invasion and migration. The interaction between uroplakin 1B (UPK1B) and PI3K inhibitor interacting protein 1 (PIK3IP1) was experimentally validated. A set of prognostic signature genes associated with the malignant metastasis of GC was identified, among which UPK1B and chorionic gonadotropin subunit β-5 were demonstrated to be independent predictors of a poor outcome. Notably, UPK1B was validated as an independent biomarker of poor prognosis and a potential therapeutic target in GC. Functional experiments revealed that UPK1B interacted with PIK3IP1 and attenuated the inhibitory effect of PIK3IP1 on the PI3K/AKT signaling pathway, thereby enhancing GC cell invasion and migration. In addition, caudal-related homeobox transcription factor 2 (CDX2) was identified as the transcriptional repressor of UPK1B. The present study delineated prognostic signature genes associated with malignant metastasis of GC. Among them, UPK1B served a pivotal role in regulating GC cell invasion and migration via the CDX2-UPK1B-PIK3IP1-PI3K/AKT axis. These findings provide novel insights into the molecular mechanisms underlying GC metastasis, and highlight UPK1B as a promising biomarker and therapeutic target for future GC therapies.

Correspondence to: Dr Jin Huang, Gastroenterology/Endoscopy Clinic, The First Affiliated Hospital of University of Science and Technology of China (Anhui Provincial Tumor Hospital), Division of Life Science and Medicine, University of Science and Technology of China, 107 Huan Hu Road, Hefei, Anhui 230031, P.R. China
E-mail: huangjinslyy@163.com

Key words: gastric cancer, uroplakin 1B, caudal-related homeobox transcription factor 2, invasion, migration

Introduction

Gastric cancer (GC) remains one of the leading causes of cancer-related mortality worldwide, with malignant metastasis being a key determinant of patient prognosis (1,2). Lymph node and distant metastases are associated with advanced disease stages, treatment resistance and overall survival in patients with GC (1,2). The metastatic nature of GC also contributes to its therapeutic refractoriness and clinical complexity (1-3). Therefore, a comprehensive understanding of the molecular mechanisms underlying GC metastasis is key for the development of effective therapeutic strategies. Tumor metastasis is a multifactorial process involving aberrant cell proliferation, epithelial-mesenchymal transition (EMT), invasion, migration and immune evasion (4,5). Accordingly, molecular biomarkers that capture the metastatic potential of GC may improve risk stratification and guide personalized therapeutic decision-making (2,6).

Uroplakin 1B (UPK1B) is a glycoprotein primarily expressed on the surface of urothelial cells and belongs to the tetraspanin-like transmembrane protein family (7). The role of UPK1B in tumor progression and metastasis has attracted increasing attention (7-11). Members of the tetraspanin family are broadly implicated in tumorigenesis and metastasis. For example, CD36 is highly expressed in early-stage melanoma, whereas CD82 expression is downregulated in

metastatic prostate cancer (7). In small-cell lung cancer, UPK1B promotes stemness and invasiveness through activation of the cellular-Myc/Sox4 axis (10). In GC, a number of studies have identified UPK1B as a marker of poor prognosis (8,9,11) and chemoresistance (9), supporting its role as an independent biomarker of aggressive disease. However, the molecular mechanisms by which UPK1B promotes metastatic progression (10) in GC remain largely unexplored.

PI3K inhibitor interacting protein 1 (PIK3IP1) is a transmembrane protein that acts as a negative regulator of the PI3K/AKT signaling pathway, a key pathway in cancer initiation, progression and metastasis (12,13). PIK3IP1 shares structural homology with the PI3K p85 regulatory subunit and inhibits PI3K activity by directly binding to its p110 catalytic subunit, thereby blocking downstream AKT activation. In immune cells, PIK3IP1 suppresses PI3K signaling and T-cell activation (12,14). PIK3IP1 expression is frequently downregulated in tumors, and its overexpression suppresses tumor cell proliferation and migration (13,14). In GC, PIK3IP1 has been shown to mediate the growth-inhibitory effects of the PI3K inhibitor BYL719 (12), and similar suppression of PI3K/AKT signaling by PIK3IP1 has been reported in hepatocellular carcinoma (15). These observations support the tumor-suppressive role of PIK3IP1 in PI3K/AKT-driven malignancies.

Caudal-related homeobox transcription factor 2 (CDX2) is a transcription factor encoded by a caudal-type homeobox gene, and serves a key role in intestinal epithelial cell differentiation and development. Reduced CDX2 expression is associated with poor prognosis of patients with GC (16,17). Conversely, high CDX2 expression suppresses GC cell proliferation, invasion and migration, reduces multidrug resistance to chemotherapy, and predicts better benefit from adjuvant chemotherapy (18-20). At the mechanistic level, CDX2 has been reported to limit tumor invasiveness by inhibiting β-catenin/T-cell factor transcriptional activity (21). However, the relationship between CDX2 and UPK1B in GC remains to be fully elucidated.

Identifying key molecular markers of metastasis and investigating the role of UPK1B in GC progression are important in advancing the understanding of GC metastasis and uncovering novel therapeutic strategies. In the present study, bioinformatics approaches were employed to identify prognostic signature genes associated with poor clinical outcomes in GC, highlighting UPK1B as a key candidate for further functional and mechanistic investigation. Furthermore, the effects of UPK1B knockdown and overexpression on cell migration and invasion were assessed *in vitro*. Furthermore, molecular approaches were employed to examine putative transcriptional regulation and downstream signaling alterations.

Materials and methods

Cell culture and transfection. Human GC cell lines (AGS, HGC27, MKN45 and MKN28) and an immortalized gastric epithelial cell line (GES-1) were obtained from the Cell Bank of Type Culture Collection of The Chinese Academy of Sciences, and were subsequently authenticated by short tandem repeat profiling and routinely tested for mycoplasma contamination, with only mycoplasma-negative cultures used for experiments. All cell lines were maintained in RPMI-1640 medium (HyClone™; Cytiva) supplemented with 10% FBS (Gibco; Thermo Fisher Scientific, Inc.) and 1% 100X penicillin-streptomycin (Gibco; Thermo Fisher Scientific, Inc.) at 37˚C in a humidified incubator containing 5% CO_2. AGS cells were pretreated with LY294002 (10 μM, dissolved in RPMI-1640 medium vehicle; cat. no. S1105; Selleck Chemicals) at 37˚C for 1 h and then maintained in LY294002-containing medium for subsequent assays. LY294002 was present throughout the wound-healing and Transwell migration/invasion assays (24 h), and for pathway validation, cells were cultured under the same treatment conditions at 37˚C and harvested for western blotting of PI3K/AKT signaling proteins.

For gene knockdown experiments, cells were transfected with a GV493 short hairpin RNA (sh) plasmid targeting UPK1B (Table SI) or a negative control scrambled plasmid (sh-NC), both obtained from GeneChem, Inc. Cells were also transfected with small interfering RNAs (siRNAs) targeting CDX2 or PIK3IP1 (Table SI), with a universal non-targeting scrambled siRNA (si-NC) as the negative control (Table SI), obtained from GeneChem, Inc. For UPK1B and CDX2 overexpression, the p-TSB-CMV-UPK1B and p-TSB-CMV-CDX2 expression vectors [Shanghai Genomeditech Co., Ltd.] and the corresponding empty p-TSB-CMV vector (negative control) were used. Transfection was carried out using Lipofectamine™ 2000 (Thermo Fisher Scientific, Inc.) according to the manufacturer's instructions. For plasmid transfection (overexpression vectors), 2.5 μg of plasmid DNA was used per well (in 6-well plates), whereas for siRNA transfection, the final concentration of siRNA was 50 nM. The transfection mixture was incubated with the cells at 37˚C for 6 h, after which the medium was replaced with fresh complete medium. Functional assays and western blotting were performed at 48 h post-transfection. Lentiviral particles were generated using a second-generation packaging system. 293T cells (Cell Bank of Type Culture Collection of The Chinese Academy of Sciences) were co-transfected with 20 μg of the GV493-based shRNA plasmids (Shanghai GeneChem Co., Ltd.) and 10 μg of the Lenti-Easy Packaging Mix (containing the packaging plasmid pHelper 1.0 and the envelope plasmid pHelper 2.0; Shanghai GeneChem Co., Ltd.) using Lipofectamine™ 2000 and a plasmid ratio of 2:1. Transfection was carried out at 37˚C for 6 h. Viral supernatants were collected at 48 h post-transfection. Target cells were infected at a multiplicity of infection of 10 for 24 h. Stable cell lines were selected using puromycin starting 48 h post-infection, the concentration used was 2 μg/ml for selection and 0.5 μg/ml for maintenance. Subsequent experiments were performed 5 days after transduction.

Western blotting. Cells (GES-1, AGS, HGC27, MKN45 and MKN28) were lysed using RIPA buffer (Sigma-Aldrich; Merck KGaA) supplemented with a cOmplete™ Protease Inhibitor Cocktail (Roche Diagnostics), and protein concentrations were measured using a BCA assay kit (Thermo Fisher Scientific, Inc.). Equal amounts of protein (30 μg) were separated on 5-20% SDS-PAGE gels, followed by transfer onto PVDF membranes (MilliporeSigma). After transfer, membranes were blocked in 5% BSA (Sigma-Aldrich; Merck KGaA) dissolved in PBS for 2 h at room temperature to reduce non-specific antibody

binding. The membranes were then incubated overnight at 4˚C with primary antibodies against UPK1B, GAPDH, phosphorylated (p-)PI3K, PI3K, p-AKT, AKT and CDX2 (Table SII). Primary antibodies were generally diluted at 1:1,000, except for GAPDH (1:5,000). HRP-conjugated secondary antibodies were used at a dilution of 1:5,000. After washing in TBST (containing 0.1% Tween-20), membranes were incubated for 2 h at room temperature with HRP-conjugated secondary antibodies (Table SII). Protein bands were visualized using Tanon™ Femto-sig ECL Western Blotting Substrate (Tanon Science and Technology Co., Ltd.).

Reverse transcription-quantitative PCR (RT-qPCR). Total RNA was isolated from cultured cells using TRIzol® reagent (Invitrogen; Thermo Fisher Scientific, Inc.) according to the manufacturer's protocol. Reverse transcription was carried out using the PrimeScript RT reagent kit (Takara Biotechnology Co., Ltd.) according to the manufacturer's protocol. Furthermore, qPCR was conducted using SYBR Green Master Mix (Takara Biotechnology Co., Ltd.) on a LightCycler® 96 system (Roche Diagnostics). β-actin served as the internal reference gene. All primer sequences are listed in Table SII. The thermocycling conditions were as follows: Initial denaturation at 95˚C for 30 sec, followed by 40 cycles of denaturation at 95˚C for 5 sec and annealing/extension at 60˚C for 30 sec. A melt-curve analysis was subsequently performed to confirm the specificity of amplification. Relative mRNA expression levels were calculated using the $2^{-\Delta\Delta Cq}$ method (22).

Cell migration and invasion assays. Cell migration and invasion were assessed using Transwell chambers equipped with 8-μm pore size polycarbonate membranes (BD Biosciences). For the migration assay, uncoated chambers were used, whereas for the invasion assay, the membranes were pre-coated with Matrigel (BD Biosciences) at 37˚C for 2 h to allow matrix polymerization. GC cells were serum-starved in RPMI-1640 medium without FBS for 24 h prior to the assay. A total of $1x10^5$ cells in 0.5 ml serum-free medium were seeded into the upper chambers, while the lower chambers were filled with complete medium containing 10% FBS (Gibco; Thermo Fisher Scientific, Inc.) as a chemoattractant. After incubation for 24 h at 37˚C, non-migratory cells remaining on the upper membrane surface were gently removed using a cotton swab. Cells that had traversed to the underside of the membrane were fixed with 4% paraformaldehyde for 5 min at room temperature, stained with crystal violet for 10 min at room temperature and visualized under an inverted light microscope. Migratory or invasive cells were counted in five random fields.

Wound healing assay. GC cells were seeded into 6-well plates and cultured in complete medium until reaching 95-100% confluency. A sterile 200-μl pipette tip was used to create a linear scratch across the cell monolayer. Detached cells and debris were removed by gentle washing with serum-free medium. Cells were then maintained in serum-free medium for the remainder of the assay to minimize the influence of cell proliferation. The initial wound area was imaged under a light microscope at a magnification of x100. Subsequently, cells were incubated at 37˚C for an additional 24 h, after which images were captured again to evaluate the extent of cell migration. The relative wound closure area was quantified to assess the migratory capacity. The percentage of wound closure was calculated as follows: [(Wound area at 0 h-wound area at 24 h)/wound area at 0 h] x100.

Immunofluorescence (IF) staining. IF staining was performed on cells cultured on glass coverslips. When cells reached 30-40% confluency, they were fixed with 4% paraformaldehyde for 15 min at room temperature and permeabilized using PBS containing 0.1% Triton X-100. After blocking with 10% goat serum at room temperature for 1 h (Solarbio Science & Technology Co., Ltd.), cells were incubated overnight at 4˚C with primary antibodies against PIK3IP1 (1:100; sc-365778; Santa Cruz Biotechnology, Inc.) and UPK1B (1:100; PA5-72711; Thermo Fisher Scientific, Inc.). Subsequently, cells were incubated with the corresponding species-specific fluorescence-conjugated secondary antibodies: Goat anti-mouse IgG H&L (AF594; 1:200; 550042; ZenBio, Inc.) and goat anti-rabbit IgG H&L (AF488; 1:200; 550036; ZenBio, Inc.) for 1 h at room temperature in the dark. Nuclei were counterstained with DAPI (D9542; Sigma-Aldrich; Merck KGaA) for 10 min at room temperature. Images were acquired using a Zeiss LSM 980 confocal microscope (Zeiss GmbH).

Co-immunoprecipitation (co-IP) assay. Cells were lysed in IP Lysis Buffer (P0013; Beyotime Institute of Biotechnology) containing the cOmplete™ Protease Inhibitor Cocktail (Roche Diagnostics) on ice for 30 min. For each IP reaction, equal amounts of total protein (1 mg) were incubated with 2 μg of specific primary antibodies targeting PIK3IP1 (671477; ZenBio, Inc.) and UPK1B (PA5-72711; Thermo Fisher Scientific, Inc.) overnight at 4˚C. The next day, 30 μl of protein A/G agarose beads (sc-2003; Santa Cruz Biotechnology, Inc.) were added for incubation for an additional 6 h at 4˚C with gentle rotation. Parallel reactions using control rabbit IgG or mouse IgG (A00002 and A00001; ZenBio, Inc.) served as negative controls. After washing three times with cold IP Lysis Buffer, the immunoprecipitated complexes were collected by centrifugation at 1,000 x g for 2 min at 4˚C. The pellets were then resuspended in SDS loading buffer and boiled for 5 min before being subjected to downstream analysis through western blotting as aforementioned.

Bioinformatics analysis. RNA-sequencing data from The Cancer Genome Atlas Stomach Adenocarcinoma (TCGA-STAD) cohort were retrieved from TCGA portal (https://portal.gdc.cancer.gov) and normalized to transcripts per million (TPM) values. Gene set enrichment analysis was conducted using the 'clusterProfiler' R package version 4.4.4 (23) from R Studio version 2023.12.1 (Posit Software, PBC). Survival analysis was conducted using the Kaplan-Meier (KM) Plotter database (https://kmplot.com) [including all datasets: GSE14210 (24), GSE15459 (25), GSE22377 (26), GSE29272 (27), GSE51105 (28), GSE62254 (29)] with Auto select best cutoff percentiles. Protein-protein interaction (PPI) information for the target gene(s) was retrieved from two curated repositories: The Human Integrated Protein-Protein Interaction rEference (HIPPIE; https://cbdm-01.zdv.uni-mainz.de/~mschaefer/hippie/) and the Biological General Repository for Interaction Datasets (BioGRID; https://thebiogrid.org/).

Gene symbols (and corresponding UniProt accessions when needed) were queried using each database's web interface, restricting results to *Homo sapiens* and experimentally supported physical PPIs. Furthermore, the ChIP-X Enrichment Analysis (ChEA; https://maayanlab.cloud/Harmonizome/) and ChEA3 (https://maayanlab.cloud/chea3/) platforms were used to predict transcription factors for specific genes or gene sets.

Statistical analysis. All experiments were performed in triplicate independent replicates. Statistical analysis was conducted using GraphPad Prism (version 8.0; Dotmatics). Normally distributed data are presented as the mean ± SD. Comparisons between two groups were made using an unpaired two-tailed Student's t-test. For comparisons among ≥3 groups, one-way ANOVA followed by Tukey's post hoc test was performed. Kaplan-Meier survival curves were compared using the log-rank test, and Cox proportional hazards regression models were used for univariate and multivariate analyses of prognostic factors. $P<0.05$ was considered to indicate a statistically significant difference.

Results

Identification of a metastasis-related prognostic signature in GC. Lymph node and distant metastases are two major manifestations of GC dissemination (30). To identify genes associated with these traits, differential expression analysis between tumors with and without lymph node involvement (N0 vs. N1-3) and with and without distant metastasis (M0 vs. M1) was performed based on TCGA-STAD RNA-seq dataset. Genes with $\log_2$(fold change) >0.585 and adjusted $P<0.05$ were considered significant. The intersection of these two gene sets yielded 26 upregulated genes involved in both lymphatic and distant metastases of GC cells (Table SIII; Fig. 1A).

Prognostic data were further obtained for the TCGA cohort, and Least Absolute Shrinkage and Selection Operator Cox regression analyses were conducted (Fig. 1B), which identified a 12-gene prognostic signature. The corresponding risk score formula was defined as follows: Risk score=(0.0710) x UPK1B + (0.0911) x TFPI2 + (0.0372) x IL6 + (0.1959) x ST8SIA6-(0.0546) x LGALS9C + (0.0244) x PSAPL1 + (0.3766) x SYT16-(0.1152) x DCHS2 + (0.1222) x IRS4 + (0.0024) x VMO1 + (0.0082) x UPK2 + (0.1254) x chorionic gonadotropin subunit β-5 (CGB5). Survival analysis using TCGA-STAD data demonstrated that patients with higher risk scores exhibited a significantly poorer prognosis (Fig. 1C). Cox regression analysis was also performed on the 26 metastasis-related genes, identifying eight genes as potential prognostic factors after univariate analysis (Table SIV) and two genes, UPK1B and CGB5, as independent prognostic factors after multivariate analysis (Table SIV). Fig. 1D and E show that high expression of UPK1B and CGB5 is significantly associated with diminished overall survival in patients with GC in TCGA-STAD dataset. Collectively, these analyses defined a metastasis-related 12-gene prognostic signature, and highlighted UPK1B and CGB5 as independent prognostic markers in GC, providing a basis for risk stratification of patients with advanced disease.

Consistent with the signature-based findings, in the TCGA-STAD cohort and KM Plotter database, higher UPK1B expression was associated with shorter overall survival (Fig. 1E and F), and UPK1B levels were significantly increased in tumors with distant (M1) and advanced nodal (N2) metastasis compared to those with M0 and N0 status, respectively (Fig. 1G and H). As CGB5 has been extensively studied in gastric cancer (31-34), the present analysis was focused on UPK1B to avoid redundancy and highlight novelty. These data indicated that UPK1B marked a clinically high-risk, highly metastatic subset of GC, and supported its selection for subsequent mechanistic studies.

UPK1B promotes the invasion and migration of GC cells via activation of the PI3K/AKT pathway. To explore the mechanism linking UPK1B to GC metastasis, transcriptomes of UPK1B high- and low-expression tumors in the TCGA-STAD cohort were compared. Genes in the PI3K/AKT signaling pathway were significantly enriched among those upregulated in the UPK1B high-expression group (Fig. 2A), implicating UPK1B in PI3K/AKT activation.

UPK1B expression was first assessed across a number of GC cell lines, with the highest levels observed in MKN45 and the lowest in AGS (Fig. 2B). UPK1B knockdown in MKN45 cells reduced PI3K/AKT phosphorylation (Fig. 2C), and markedly decreased invasion and migration (Fig. 2D and E), whereas UPK1B overexpression in AGS cells enhanced PI3K/AKT activation (Fig. 2F), and increased the invasive and migratory capacity (Fig. 2G and H). Notably, the PI3K/AKT inhibitor LY294002 (10 μM) abrogated the pro-invasive and pro-migratory effects of UPK1B overexpression (Fig. 2F-H), demonstrating that UPK1B-driven metastatic phenotypes are PI3K/AKT-dependent. Together, these findings suggested UPK1B as a functional driver of GC cell invasion and migration through activation of the PI3K/AKT pathway, and indicated that tumors with high UPK1B expression may be particularly sensitive to PI3K/AKT-targeted therapies.

UPK1B attenuates the inhibitory effect of PIK3IP1 on PI3K/AKT signaling. To investigate how UPK1B activates PI3K/AKT signaling, HIPPIE and BioGRID interaction databases were interrogated, and PIK3IP1, a negative regulator of PI3K, was identified as a putative UPK1B binding partner (Fig. 3A; Table SV). Consistently, IF staining showed co-localization of UPK1B and PIK3IP1 at the plasma membrane (Fig. 3B), and co-IP assays demonstrated their physical interaction in MKN45 cells (Fig. 3C).

Dual knockdown experiments demonstrated that silencing of PIK3IP1 in UPK1B-deficient MKN45 cells (Fig. 3D) restored PI3K/AKT activation (Fig. 3E), and improved invasion and migration (Fig. 3F and G). These data support a model in which UPK1B promotes PI3K/AKT signaling and pro-metastatic behavior by functionally antagonizing the inhibitory regulator PIK3IP1. Therefore, by releasing PI3K from PIK3IP1-mediated restraint, UPK1B may amplify PI3K/AKT signaling in high-risk GC, providing a mechanistic rationale for targeting this axis in patients with UPK1B upregulation.

CDX2 suppresses UPK1B expression. To identify upstream regulators responsible for UPK1B upregulation during invasion and migration, the top 20 predicted transcription factors

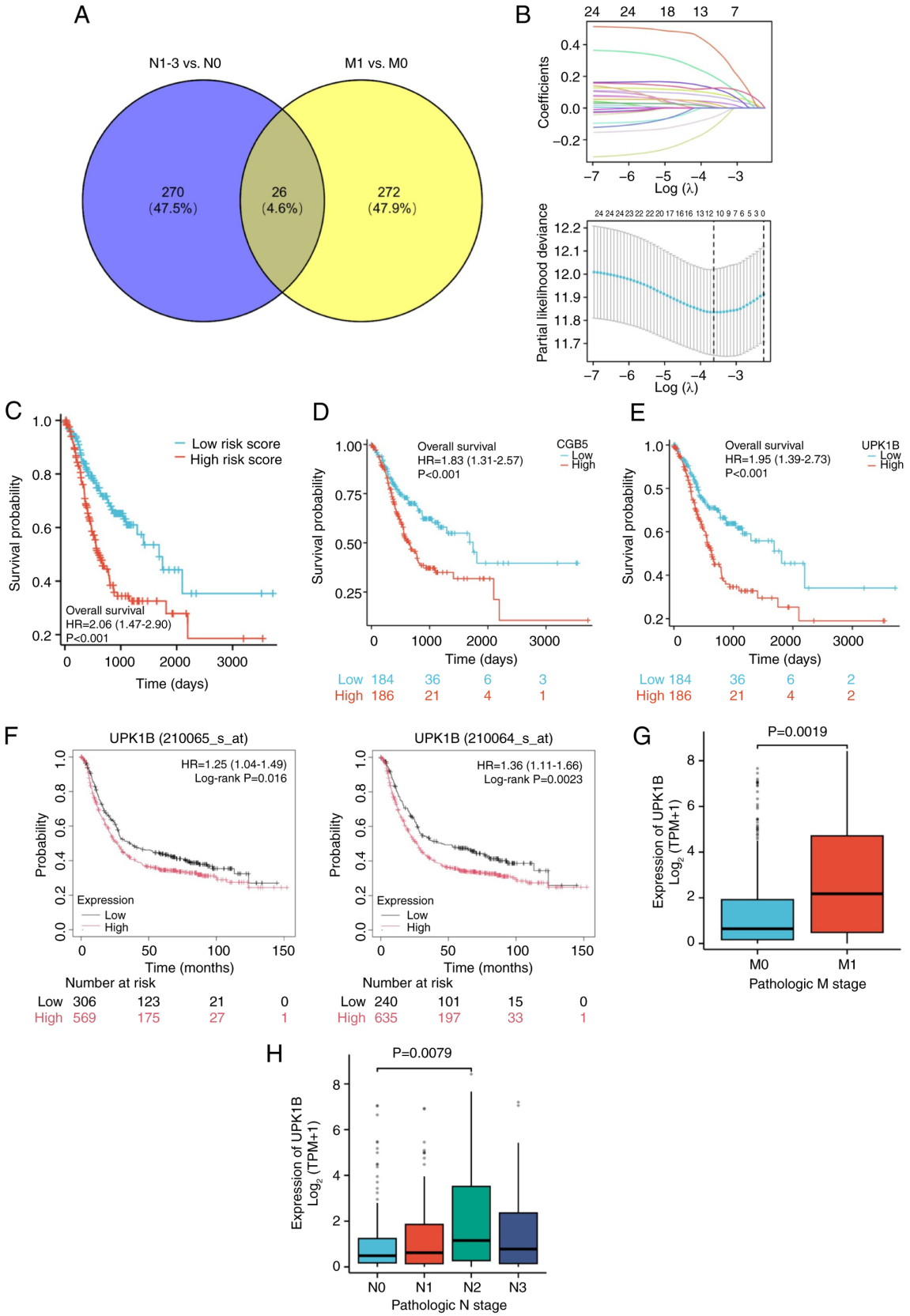

Figure 1. Metastasis-related 12-gene signature, and identification of UPK1B and CGB5 as independent prognostic markers associated with advanced metastatic GC. (A) Venn diagram showing the intersection of genes upregulated in N1-3 stage and M1 stage GC tissues. (B) LASSO Cox regression analysis based on TCGA-STAD data identified a metastasis-associated prognostic risk signature. LASSO coefficient profiles of the signature genes in the merged dataset are shown (top) and the coefficient profile plot is generated against the log(λ) sequence (bottom). (C) The high-risk group of patients with GC exhibited a poor prognosis (overall survival). High expression of (D) CGB5 and (E) UPK1B was associated with poor overall survival in patients with GC based on data from the TCGA-STAD cohort. (F) Elevated UPK1B expression predicted poor prognosis (overall survival) of patients with GC in the Kaplan-Meier plotter database. UPK1B expression was increased in (G) M1 compared with M0 and in (H) N2 metastatic stage GC tissues compared with N0 stage. UPK1B, uroplakin 1B; CGB5, chorionic gonadotropin subunit β-5; GC, gastric cancer; LASSO, Least Absolute Shrinkage and Selection Operator; TCGA-STAD, The Cancer Genome Atlas Stomach Adenocarcinoma; HR, hazard ratio; TPM, transcripts per million.

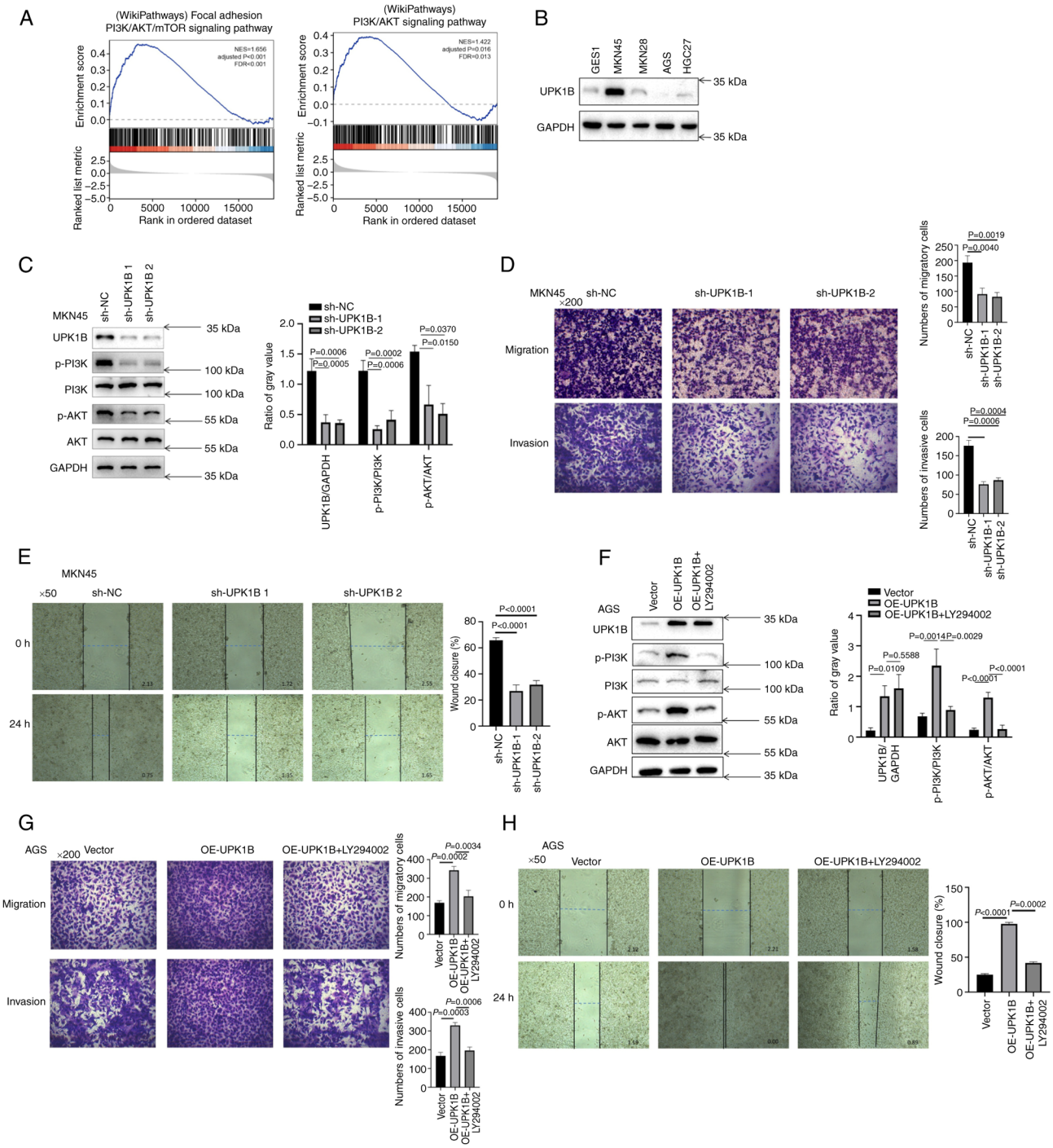

Figure 2. UPK1B drives GC cell invasion and migration in a PI3K/AKT-dependent manner. (A) Gene set enrichment analysis indicated that genes upregulated in the UPK1B-high group were enriched in the PI3K/AKT pathway. (B) Protein levels of UPK1B in GC cell lines. (C) Knockdown of UPK1B reduced PI3K/AKT activation in MKN45 cells. Silencing UPK1B suppressed the (D) migration/invasion capacity and (E) wound closure rate of MKN45 cells. (F) Overexpression of UPK1B enhanced PI3K/AKT pathway activation in AGS cells, which was attenuated by the PI3K inhibitor LY294002. Inhibition of PI3K/AKT signaling reversed UPK1B-induced (G) migration/invasion capacity and (H) wound closure rate of AGS cells. UPK1B, uroplakin 1B; GC, gastric cancer; p-, phosphorylated; sh, short hairpin RNA; NC, negative control; OE, overexpression.

(ESR1 and SOX2 appeared twice) (Table SVI) regulating UPK1B were first retrieved using the ChEA platform within Harmonizome. The ChEA3 platform was then employed to predict the top 20 upstream transcription factors (Table SVII) for the genes co-expressed with UPK1B (R>0.4; adjusted P<0.05) based on TCGA-STAD dataset. CDX2 emerged as the top-ranking transcription factor for these co-expressed genes (Table SVII), and the intersection of both analyses (Fig. 4A) suggested that CDX2 acts as an upstream transcriptional regulator of UPK1B.

Consistent with this prediction, CDX2 knockdown in AGS cells (Fig. 4B) increased UPK1B mRNA and protein expression (Fig. 4C and D), whereas CDX2 overexpression in MKN45 cells reduced UPK1B protein levels (Fig. 4E). Clinical data from TCGA-STAD and the KM Plotter database further showed that low CDX2 expression in GC tissues was

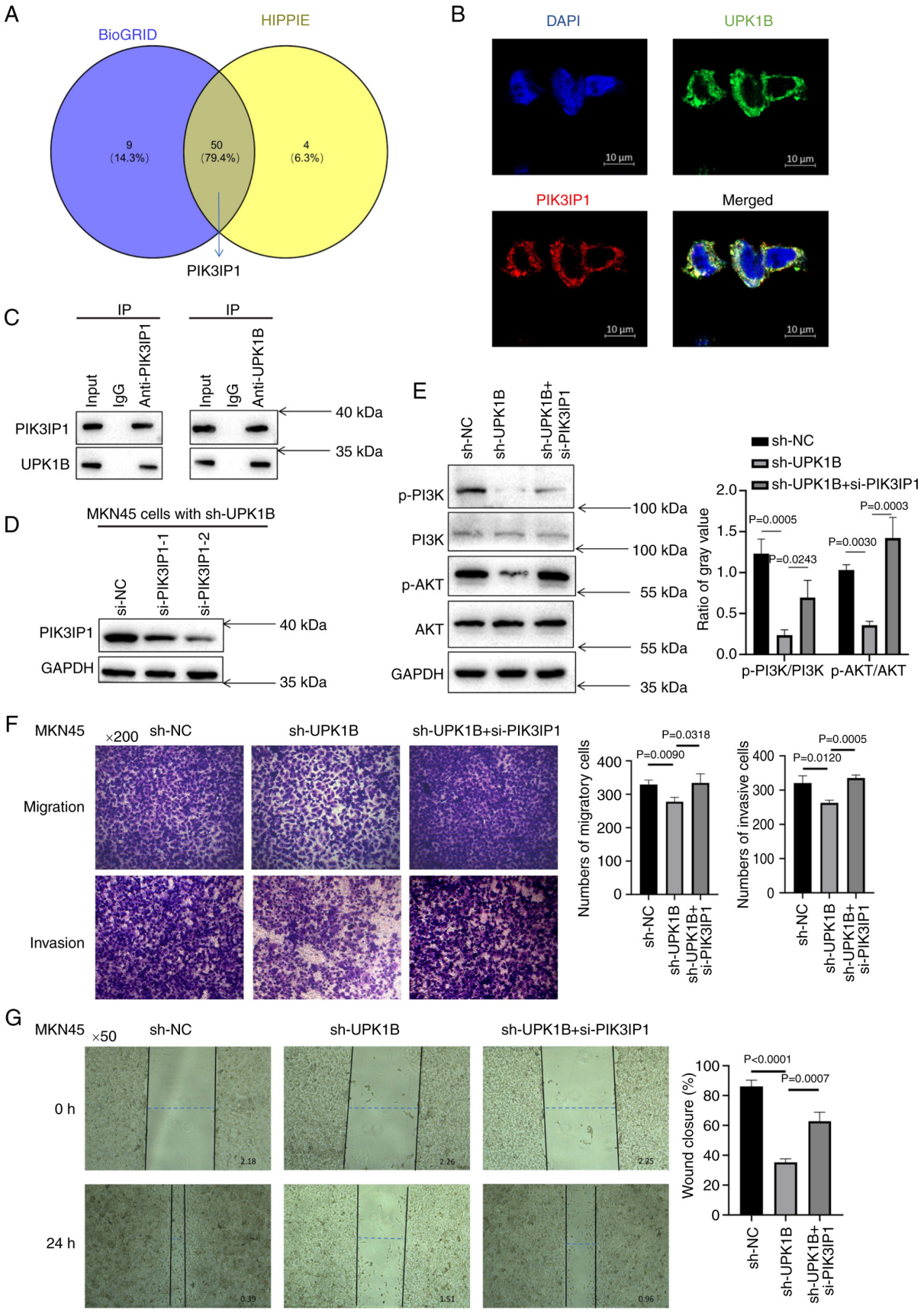

Figure 3. UPK1B activates PI3K/AKT signaling by antagonizing the inhibitory regulator PIK3IP1 in gastric cancer cells. (A) Venn diagram showing that PIK3IP1 was identified as a putative UPK1B-interacting partner based on BioGRID and HIPPIE protein-protein interaction databases. (B) UPK1B and PIK3IP1 co-localized in the cytoplasm and plasma membrane of MKN45 cells. (C) Interaction between UPK1B and PIK3IP1 in MKN45 cells. (D) Knockdown of PIK3IP1 in MKN45 cells. (E) Silencing PIK3IP1 in UPK1B-knockdown MKN45 cells restored PI3K/AKT pathway activation. Knockdown of PIK3IP1 reversed the decrease in (F) migration/invasion and (G) wound-healing capacity in UPK1B-silenced MKN45 cells. UPK1B, uroplakin 1B; p-, phosphorylated; si, small interfering RNA; sh, short hairpin RNA; NC, negative control; PIK3IP1, PI3K inhibitor interacting protein 1; HIPPIE, Human Integrated Protein-Protein Interaction Reference; IP, immunoprecipitation.

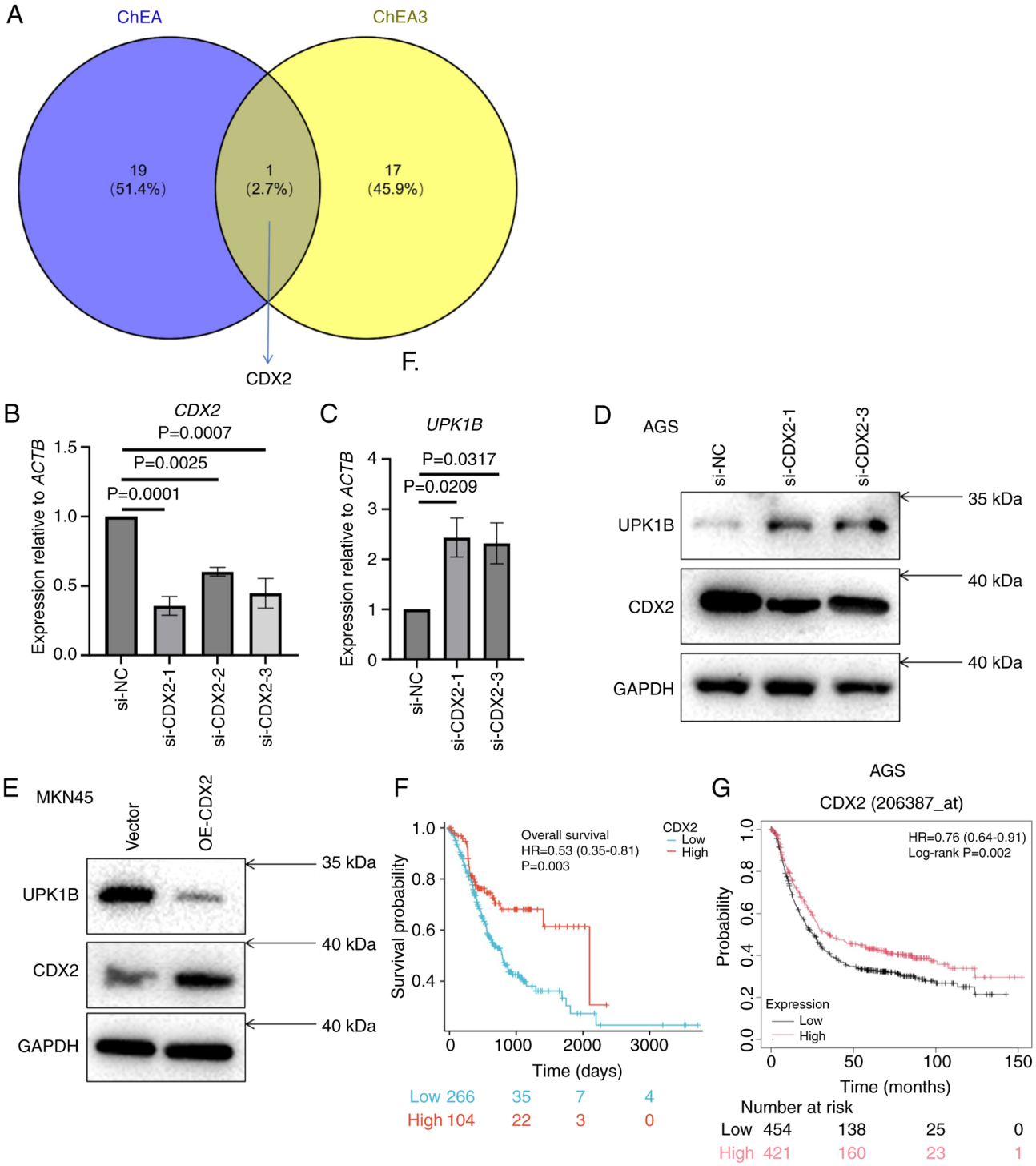

Figure 4. CDX2 acts as a transcriptional repressor of UPK1B and its high expression is associated with favorable prognosis of patients with GC. (A) Venn diagram showing overlapping predicted transcriptional regulators of UPK1B from ChEA and ChEA3 databases. (B) Knockdown of CDX2 in AGS cells resulted in increased UPK1B (C) mRNA and (D) protein expression. (E) Overexpression of CDX2 in MKN45 cells reduced UPK1B protein levels. Data from (F) The Cancer Genome Atlas Stomach Adenocarcinoma cohort and (G) the Kaplan-Meier plotter database indicated that high CDX2 expression was associated with improved prognosis of patients with GC. UPK1B, uroplakin 1B; GC, gastric cancer; si, small interfering RNA; NC, negative control; OE, overexpression; HR, hazard ratio; CDX2, caudal-related homeobox transcription factor 2; ChEA, ChIP-X Enrichment Analysis.

associated with a poorer prognosis compared with that in the high CDX2 group (Fig. 4F and G). These findings indicated that loss of the tumor-suppressive transcription factor CDX2 could de-repress UPK1B, thereby associating CDX2 downregulation with the activation of the UPK1B-PIK3IP1-PI3K/AKT axis and the adverse clinical outcomes observed in GC.

Discussion

Through integrated bioinformatics analyses and cellular experiments, two independent prognostic genes, CGB5 and UPK1B, were identified, and a novel regulatory axis, CDX2-UPK1B-PIK3IP1-PI3K/AKT, which promotes GC

migration and invasion, was revealed. This axis elucidates the molecular basis of UPK1B upregulation during GC progression and its contribution to poor clinical outcomes, providing a mechanistic framework associating distinct molecular alterations with metastatic behavior and patient prognosis.

CGB5 has previously been reported as a prognostic marker whose high expression is associated with poor prognosis, particularly in advanced GC (31,32). Consistently, a number of studies have shown that elevated UPK1B expression is associated with poor prognosis in patients with GC (8,9,11). UPK1B encodes a membrane-associated protein that forms a heterotetrameric complex with Upk1a, Upk2 and Upk3 in normal urothelial cells (35). However, its functional status, ligand interactions and downstream signaling mechanisms on the surface of tumor cells remain poorly understood. Its potential ligands may include cell adhesion molecules or extracellular matrix proteins such as collagen and fibronectin (36,37). In this context, high UPK1B expression could potentially indicate intrinsic or acquired resistance to standard chemotherapy, and patients with tumors with high UPK1B expression may preferentially benefit from therapeutic strategies that combine cytotoxic agents with PI3K/AKT pathway inhibitors (9,38,39). Thus, UPK1B emerges as both a prognostic biomarker and a putative predictor of therapeutic response in GC.

UPK1B is implicated in chemoresistance in GC (9). Given that activation of the PI3K/AKT pathway is a known driver of chemoresistance and that combining chemotherapeutic agents with PI3K/AKT inhibitors enhances drug efficacy (40,41), UPK1B may promote chemoresistance, at least in part, through PI3K/AKT signaling. This suggests the therapeutic potential of UPK1B inhibitors, or their combination with PI3K/AKT inhibitors, in overcoming drug resistance.

Class I PI3Ks, which are widely expressed in immune cells, consist of a regulatory subunit (p85) and a catalytic subunit (p110) (42). Upon T-cell receptor activation, the SH2 domains of p85 mediate membrane recruitment of PI3K, allowing p110 to phosphorylate phosphatidylinositol (4,5)-bisphosphate (PIP2) to generate phosphatidylinositol (3,4,5)-trisphosphate (PIP3). PI3K activity is modulated by numerous upstream signals, including the cytokine receptor-Janus kinase (JAK)/STAT axis (43), receptor tyrosine kinases (44) and G protein-coupled receptors (45,46). Conversely, a number of negative regulators such as PTEN and inositol polyphosphate-5-phosphatase D inhibit PI3K activity by dephosphorylating PIP3, and inositol polyphosphate-4-phosphatase type II B reduces PI3K signaling by acting on PIP2 (42). Additionally, suppressor of cytokine signaling proteins suppress cytokine-mediated PI3K activation by interacting with JAK kinases (47).

PI3K/AKT signaling enhances GC invasion and metastasis through a number of mechanisms, including upregulation of matrix metalloproteinases, induction of EMT (48), suppression of GSK3β leading to Wnt/β-catenin pathway activation (49) and stimulation of Rho GTPases that mediate cytoskeletal remodeling (50). Furthermore, PI3K/AKT/mTOR signaling promotes immune evasion through upregulation of programmed death-ligand 1 expression (51).

The present results suggested that UPK1B may promote PI3K/AKT signaling through its interaction with PIK3IP1, a negative regulator of PI3K. PIK3IP1 contains a p85-like intracellular domain that binds the p110 catalytic subunit of PI3K, thereby suppressing its activity without disrupting p85-p110 interaction (42,52). UPK1B may disrupt the inhibitory PIK3IP1-p110 interaction through its C-terminal region, leading to enhanced PI3K activation and downstream AKT phosphorylation (42,52). Further mechanistic studies are warranted to define how UPK1B regulates PIK3IP1. These may include overexpression of membrane-localized UPK1B truncation mutants, as well as assays exploring potential roles for UPK1B in PIK3IP1 endocytosis or membrane compartmentalization. Additional experiments, including co-IP and domain-mapping, are required to delineate the precise interaction interface and its functional consequences. From a translational perspective, the UPK1B-PIK3IP1-PI3K/AKT axis may represent a druggable axis in tumors with high UPK1B expression, in which restoring PIK3IP1-mediated inhibition or directly targeting PI3K/AKT could attenuate metastatic progression and improve treatment outcomes.

CDX2, a key transcription factor in intestinal epithelial cells, is downregulated in aggressive and metastatic GC (16,53), contributing to poor clinical outcomes, consistent with the present results. CDX2 may modulate PI3K/AKT signaling through a number of mechanisms, including downregulating PTEN (54). Beyond PTEN, the present study suggested that UPK1B may represent another downstream effector of CDX2. During malignant progression, particularly in the metastatic stage, loss of CDX2 may lead to upregulation of UPK1B, thereby enhancing GC cell invasion and migration. These findings imply that concomitant assessment of CDX2 and UPK1B expression could refine prognostic stratification, distinguishing patients with more aggressive, metastasis-prone disease who might benefit from intensified surveillance and targeted inhibition of the CDX2-UPK1B-PIK3IP1-PI3K/AKT axis.

The present study has certain limitations. Firstly, the transcriptomic and survival analyses were largely based on retrospective TCGA and publicly available datasets, which may introduce selection bias and limit generalizability. Secondly, the functional validation of UPK1B and its interaction with PIK3IP1 relied mainly on *in vitro* experiments in a limited number of GC cell lines, without further demonstration using *in vivo* models of metastatic dissemination. Thirdly, UPK1B, CDX2 and PIK3IP1 protein expression levels were not validated. Furthermore, correlations between the protein levels of UPK1B, CDX2 and PIK3IP1 in large, independent clinical cohorts or tissue microarrays were not explored. In addition, chromatin immunoprecipitation (ChIP) or promoter-reporter assays to demonstrate direct CDX2 binding to the UPK1B promoter have not been performed. Future studies should therefore aim to: i) Validate UPK1B protein expression and its relationship with CDX2 and PIK3IP1 in paired primary and metastatic GC tissues; ii) use ChIP and promoter assays to demonstrate direct transcriptional regulation of UPK1B by CDX2; and iii) employ *in vivo* models to investigate the impact of UPK1B on metastatic spread, and on the response to chemotherapy and PI3K/AKT-targeted therapies.

In conclusion, the present study identified metastasis-related prognostic genes in GC, and demonstrated that UPK1B and CGB5 were independent prognostic markers associated with advanced metastatic stage and poor survival. Mechanistically, a CDX2-UPK1B-PIK3IP1-PI3K/AKT

signaling axis, which drives GC cell invasion and migration, was uncovered. Clinically, the present findings suggest that UPK1B, particularly in combination with CDX2 and CGB5, may be useful for prognostic stratification, for selecting patients who are more likely to benefit from PI3K/AKT-targeted strategies. These results highlight the CDX2-UPK1B-PIK3IP1-PI3K/AKT axis as a promising biomarker and potential therapeutic target in metastatic GC.

Acknowledgements

Not applicable.

Funding

No funding was received.

Availability of data and materials

The data generated in the present study may be requested from the corresponding author.

Authors' contributions

SZ designed the present study, conducted the experiments, analyzed data and wrote the manuscript. HZ analyzed data and wrote the manuscript. JH was responsible for project conception, study design and revisions to the manuscript. SZ and JH confirm the authenticity of all the raw data. All authors have read and approved the final manuscript.

Ethics approval and consent to participate

Not applicable.

Patient consent for publication

Not applicable.

Competing interests

The authors declare that they have no competing interests.

References

1. Luo D, Zhou J, Ruan S, Zhang B, Zhu H, Que Y, Ying S, Li Y, Hu Y and Song Z: Overcoming immunotherapy resistance in gastric cancer: Insights into mechanisms and emerging strategies. Cell Death Dis 16: 75, 2025.
2. Burz C, Pop V, Silaghi C, Lupan I and Samasca G: Prognosis and treatment of gastric cancer: A 2024 update. Cancers (Basel) 16: 1708, 2024.
3. Lee JE, Kim KT, Shin SJ, Cheong JH and Choi YY: Genomic and evolutionary characteristics of metastatic gastric cancer by routes. Br J Cancer 129: 672-682, 2023.
4. Matsuoka T and Yashiro M: Molecular insight into gastric cancer invasion-current status and future directions. Cancers (Basel) 16: 54, 2023.
5. Wang G, Xu D, Zhang Z, Li X, Shi J, Sun J, Liu HZ, Li X, Zhou M and Zheng T: The pan-cancer landscape of crosstalk between epithelial-mesenchymal transition and immune evasion relevant to prognosis and immunotherapy response. NPJ Precis Oncol 5: 56, 2021.
6. Sun Y., P. Puspanathan T. Lim, and D. Lin, Advances and challenges in gastric cancer testing: the role of biomarkers. Cancer Biol Med 22: 212-230, 2025.
7. Finch JL, Webb GC, Evdokiou A and Cowled PA: Chromosomal localization of the human urothelial 'tetraspan' gene, UPK1B, to 3q13.3-q21 and detection of a TaqI polymorphism. Genomics 40: 501-503, 1997.
8. Zhu Z, Xu J, Li L, Ye W, Chen B, Zeng J and Huang Z: Comprehensive analysis reveals CTHRC1, SERPINE1, VCAN and UPK1B as the novel prognostic markers in gastric cancer. Transl Cancer Res 9: 4093-4110, 2020.
9. Zhang Y, Yuan Z, Shen R, Jiang Y, Xu W, Gu M and Gu X: Identification of biomarkers predicting the chemotherapeutic outcomes of capecitabine and oxaliplatin in patients with gastric cancer. Oncol Lett 20: 290, 2020.
10. Liu Y, Ding L, Li C, Heng L, Chen J and Hou Y: UPK1B promoted the invasion and stem cell characteristics of non-small cell lung cancer cells by modulating c-myc/Sox4 axis. Tissue Cell 85: 102250, 2023.
11. Dai J, Li ZX, Zhang Y, Ma JL, Zhou T, You WC, Li WQ and Pan KF: Whole genome messenger RNA profiling identifies a novel signature to predict gastric cancer survival. Clin Transl Gastroenterol 10: e00004, 2019.
12. Ma XB, Wang Y, Jia YJ, Liu YJ, Tian YQ, Liu Y, Hou GQ, Xu YC and Liu HM: Upregulation of PIK3IP1 monitors the anti-cancer activity of PI3Kα inhibitors in gastric cancer cells. Biochem Pharmacol 207: 115380, 2023.
13. Jia Y, He P, Ma X, Lv K, Liu Y and Xu Y: PIK3IP1: Structure, aberration, function, and regulation in diseases. Eur J Pharmacol 977: 176753, 2024.
14. DeFrances MC, Debelius DR, Cheng J and Kane LP: Inhibition of T-cell activation by PIK3IP1. Eur J Immunol 42: 2754-2759, 2012.
15. He X, Zhu Z, Johnson C, Stoops J, Eaker AE, Bowen W and DeFrances MC: PIK3IP1, a negative regulator of PI3K, suppresses the development of hepatocellular carcinoma. Cancer Res 68: 5591-5598, 2008.
16. Masood MA, Loya A and Yusuf MA: CDX2 as a prognostic marker in gastric cancer. Acta Gastroenterol Belg 79: 197-200, 2016.
17. Khayyat A, Pour MA, Poursina O, Zohouri SA, Jian PV, Patel N and Amin A: Evaluations of biomarkers CDX1 and CDX2 in gastric cancer prognosis: A meta-analysis. Int J Mol Cell Med 13: 1-19, 2024.
18. Xie Y, Li L, Wang X, Qin Y, Qian Q, Yuan X and Xiao Q: Overexpression of Cdx2 inhibits progression of gastric cancer in vitro. Int J Oncol 36: 509-516, 2010.
19. Gao X, Han W, Chen L, Li H, Zhou F, Bai B, Yan J, Guo Y, Liu K and Li W: Association of CDX2 and mucin expression with chemotherapeutic benefits in patients with stage II/III gastric cancer. Cancer Med 12: 17613-17631, 2023.
20. Yan LH, Wang XT, Yang J, Lian C, Kong FB, Wei WY, Luo W, Xiao Q and Xie YB: Reversal of multidrug resistance in gastric cancer cells by CDX2 downregulation. World J Gastroenterol 19: 4155-4165, 2013.
21. Guo RJ, Funakoshi S, Lee HH, Kong J and Lynch JP: The intestine-specific transcription factor Cdx2 inhibits beta-catenin/TCF transcriptional activity by disrupting the beta-catenin-TCF protein complex. Carcinogenesis 31: 159-166, 2010.
22. Livak KJ and Schmittgen TD: Analysis of relative gene expression data using real-time quantitative PCR and the 2(-Delta Delta C(T)) method. Methods 25: 402-408, 2001.
23. Yu G, Wang LG, Han Y and He QY: clusterProfiler: An R package for comparing biological themes among gene clusters. OMICS 16: 284-287, 2012.
24. Kim HK, Choi IJ, Kim CG, Kim HS, Oshima A, Michalowski A and Green JE: A gene expression signature of acquired chemoresistance to cisplatin and fluorouracil combination chemotherapy in gastric cancer patients. PLoS One 6: e16694, 2011.
25. Ooi CH, Ivanova T, Wu J, Lee M, Tan IB, Tao J, Ward L, Koo JH, Gopalakrishnan V, Zhu Y, *et al*: Oncogenic pathway combinations predict clinical prognosis in gastric cancer. PLoS Genet 5: e1000676, 2009.
26. Förster S, Gretschel S, Jöns T, Yashiro M and Kemmner W: THBS4, a novel stromal molecule of diffuse-type gastric adenocarcinomas, identified by transcriptome-wide expression profiling. Mod Pathol 24: 1390-1403, 2011.

27. Wang G, Hu N, Yang HH, Wang L, Su H, Wang C, Clifford R, Dawsey EM, Li JM, Ding T, *et al*: Comparison of global gene expression of gastric cardia and noncardia cancers from a high-risk population in china. PLoS One 8: e63826, 2013.
28. Busuttil RA, George J, Tothill RW, Ioculano K, Kowalczyk A, Mitchell C, Lade S, Tan P, Haviv I and Boussioutas A: A signature predicting poor prognosis in gastric and ovarian cancer represents a coordinated macrophage and stromal response. Clin Cancer Res 20: 2761-2772, 2014.
29. Cristescu R, Lee J, Nebozhyn M, Kim KM, Ting JC, Wong SS, Liu J, Yue YG, Wang J, Yu K, *et al*: Molecular analysis of gastric cancer identifies subtypes associated with distinct clinical outcomes. Nat Med 21: 449-456, 2015.
30. Verstegen MH, Harker M, van de Water C, van Dieren J, Hugen N, Nagtegaal ID, Rosman C and van der Post RS: Metastatic pattern in esophageal and gastric cancer: Influenced by site and histology. World J Gastroenterol 26: 6037-6046, 2020.
31. Yang Y, Shi Y, Hou Y, Lu Y and Yang J: CGB5 expression is independently associated with poor overall survival and recurrence-free survival in patients with advanced gastric cancer. Cancer Med 7: 716-725, 2018.
32. Ji B, Qiao L and Zhai W: CGB5, INHBA and TRAJ19 hold prognostic potential as immune genes for patients with gastric cancer. Dig Dis Sci 68: 791-802, 2023.
33. Chen S, Lin S, Li F, He H, Zhang Y, Ma G and Yu W: Comprehensive pan-cancer analysis reveals CGB5 is a potential promising predictive and immunotherapeutic biomarker. Front Med (Lausanne) 12: 1624815, 2025.
34. Gao F, Zhou X, Wei J, Sun Q, Wang J and Li Q: Expression characteristics and biological functions of CGB5 gene in gastric cancer. Acta Histochem 127: 152254, 2025.
35. Carpenter AR, Becknell MB, Ching CB, Cuaresma EJ, Chen X, Hains DS and McHugh KM: Uroplakin 1b is critical in urinary tract development and urothelial differentiation and homeostasis. Kidney Int 89: 612-624, 2016.
36. Berditchevski F: Complexes of tetraspanins with integrins: More than meets the eye. J Cell Sci 114: 4143-4151, 2001.
37. Hemler ME: Tetraspanin functions and associated microdomains. Nat Rev Mol Cell Biol 6: 801-811, 2005.
38. Zhu H, Jiang W, Zhang Q and Yu C: The role of UPK1B in gastric cancer: Multi-omics analysis and experimental validation. Discov Oncol 16: 476, 2025.
39. Kim KJ, Kim JW, Sung JH, Suh KJ, Lee JY, Kim SH, Lee JO, Kim JW, Kim YJ, Kim JH, *et al*: PI3K-targeting strategy using alpelisib to enhance the antitumor effect of paclitaxel in human gastric cancer. Sci Rep 10: 12308, 2020.
40. Matsuoka T and Yashiro M: The role of PI3K/Akt/mTOR signaling in gastric carcinoma. Cancers (Basel) 6: 1441-1463, 2014.
41. Almhanna K, Strosberg J and Malafa M: Targeting AKT protein kinase in gastric cancer. Anticancer Res 31: 4387-4392, 2011.
42. Uche UU, Piccirillo AR, Kataoka S, Grebinoski SJ, D'Cruz LM and Kane LP: PIK3IP1/TrIP restricts activation of T cells through inhibition of PI3K/Akt. J Exp Med 215: 3165-3179, 2018.
43. Lu Y, Zhou J, Xu C, Lin H, Xiao J, Wang Z and Yang B: JAK/STAT and PI3K/AKT pathways form a mutual transactivation loop and afford resistance to oxidative stress-induced apoptosis in cardiomyocytes. Cell Physiol Biochem 21: 305-314, 2008.
44. Haddadi N, Lin Y, Travis G, Simpson AM, Nassif NT and McGowan EM: PTEN/PTENP1: 'Regulating the regulator of RTK-dependent PI3K/Akt signalling', new targets for cancer therapy. Mol Cancer 17: 37, 2018.
45. Obata T, Yaffe MB, Leparc GG, Piro ET, Maegawa H, Kashiwagi A, Kikkawa R and Cantley LC: Peptide and protein library screening defines optimal substrate motifs for AKT/PKB. J Biol Chem 275: 36108-3615, 2000.
46. Law NC, White MF and Hunzicker-Dunn ME: G protein-coupled receptors (GPCRs) That signal via protein kinase A (PKA) cross-talk at insulin receptor substrate 1 (IRS1) to activate the phosphatidylinositol 3-kinase (PI3K)/AKT pathway. J Biol Chem 291: 27160-27169, 2016.
47. Yoshimura A, Naka T and Kubo M: SOCS proteins, cytokine signalling and immune regulation. Nat Rev Immunol 7: 454-465, 2007.
48. Xu W, Yang Z and Lu N: A new role for the PI3K/Akt signaling pathway in the epithelial-mesenchymal transition. Cell Adh Migr 9: 317-324, 2015.
49. Hermida MA, Kumar JD and Leslie NR: GSK3 and its interactions with the PI3K/AKT/mTOR signalling network. Adv Biol Regul 65: 5-15, 2017.
50. Beier F and Loeser RF: Biology and pathology of Rho GTPase, PI-3 kinase-Akt, and MAP kinase signaling pathways in chondrocytes. J Cell Biochem 110: 573-580, 2010.
51. Hudson K, Cross N, Jordan-Mahy N and Leyland R: The extrinsic and intrinsic roles of PD-L1 and Its receptor PD-1: Implications for immunotherapy treatment. Front Immunol 11: 568931, 2020.
52. Zhu Z, He X, Johnson C, Stoops J, Eaker AE, Stoffer DS, Bell A, Zarnegar R and DeFrances MC: PI3K is negatively regulated by PIK3IP1, a novel p110 interacting protein. Biochem Biophys Res Commun 358: 66-72, 2007.
53. Park DY, Srivastava A, Kim GH, Mino-Kenudson M, Deshpande V, Zukerberg LR, Song GA and Lauwers GY: CDX2 expression in the intestinal-type gastric epithelial neoplasia: Frequency and significance. Mod Pathol 23: 54-61, 2010.
54. Yu J, Li S, Xu Z, Guo J, Li X, Wu Y, Zheng J and Sun X: CDX2 inhibits epithelial-mesenchymal transition in colorectal cancer by modulation of Snail expression and β-catenin stabilisation via transactivation of PTEN expression. Br J Cancer 124: 270-280, 2021.

Copyright © 2026 Zhong et al. This work is licensed under a Creative Commons Attribution-NonCommercial-NoDerivatives 4.0 International (CC BY-NC-ND 4.0) License.